Assessment of atherosclerotic plaques in a rabbit model by multi-phase contrast-enhanced CT angiography: comparison with histopathology

Jin Hur

Department of Medicine

The Graduate School, Yonsei University

Assessment of atherosclerotic plaques in a rabbit model by multi-phase contrast-enhanced CT angiography: comparison with histopathology

Jin Hur

Department of Medicine

The Graduate School, Yonsei University

Assessment of atherosclerotic plaques in a rabbit model by multi-phase contrast-enhanced CT angiography: comparison with histopathology

Directed by Professor Byoung Wook Choi

The Doctoral Dissertation
Submitted to the Department of Medicine,
the Graduate School of Yonsei University
in partial fulfillment of the requirements
for the degree of Doctor of Philosophy

Jin Hur

December 2009

This certifies that the Doctoral Dissertation of Jin Hur is approved

Thesis Supervisor: Byoung Wook Choi

Thesis Committee Member: Kyu Ok Choe

Thesis Committee Member: Yeon Hyeon Choe

Thesis Committee Member: Hye-Yeon Lee

Thesis Committee Member: Dong Hoon Choi

The Graduate School
Yonsei University

December 2009

<Acknowledgements>

Over the past three years, many people have given me the support that has enabled me to obtain my degree. Without them, I couldn't possibly have survived the often difficult times. More importantly, it was their constructive criticism, insightful comments and refreshing perspectives on many subjects that have helped me to grow as a person. First, I would like to thank my advisor professor Byoung Wook Choi for his support and confidence in my academic ability. Second, I would like to thank professor Kyu Ok Choe, she has shown me what it takes to be a great teacher.

I am grateful to past and present staff members of our group who gave me continual advice when I was struggling with the demands of my fellowship. Many colleagues that I had known and have made while here at Severance hospital were another source of strength and consolation when I was in pain going through hard times in my fellowship. Drs. Sang Jin Kim, Tae Hoon Kim, Ji Eun Nam, Young Jin Kim, Hye-Jeong Lee, Hua Sun Kim, Yoo Jin Hong, and Sang Min Lee. Thank you all.

Last but certainly not least, I would like to thank my family for all the love and support they have given me over the past few years. Mom, Dad, Seok, my lovely wife Kyoung Hee, and my lovely kids Jun and Yoon. Thank you.

<Table of Contents>

<List of Figures>

<List of Tables>

<Abstract>

Assessment of atherosclerotic plaques in a rabbit model by multi-phase contrast-enhanced CT angiography: comparison with histopathology

Jin Hur

Department of Medicine

The Graduate School, Yonsei University

(Directed by Professor Byoung Wook Choi)

Non-invasive imaging tools that enable to detect and characterize the composition of plaques are clinically desirable. Recently, it was known that atherosclerotic plaque shows enhancement on CT angiography (CTA) after contrast administration. The purpose of this study was to assess the capability of multi-phase CTA in the characterization and quantification of atherosclerotic plaques of aorta in comparison with histopathology in an experimental rabbit model.

Twelve atherosclerotic rabbits underwent multi-phase CTA of the

abdominal aorta. The scan protocol included early phase scan (EP), delayed scan at 90 sec after contrast injection (DP_{90s}), delayed scan at 10 min after contrast injection (DP_{10min}) and delayed scan with saline infusion (DP_{Saline}). Plaque composition was analyzed according to histopathology (% of lipid-rich, fibrous and macrophage areas) and CT attenuation values (Hounsfield Unit [HU]). For each plaque, the maximum area of lumen, vessel, and plaque were measured. The correlation between CTA and histopathologic measurements was determined using Pearson's correlation coefficient.

Using histopathology as the reference standard (n=119, aortic plaques), the overall sensitivity, specificity and accuracy of 64-slice CTA for the detection of plaques were 59%, 100% and 79% for the EP scan, 88%, 100%, and 94% for the DP_{90s} scan, 81%, 100% and 90% for the DP_{10min} scan and 53%, 100% and 76% for the DP_{Saline} scan, respectively. CT density measurements were significantly different between fibrous plaques and lipid-rich plaques ($p < 0.05$). However, the CT density measurements showed substantial overlap between fibrous and lipid-rich plaques. When we divided aortic plaques into two groups according to the percentage of macrophage area using a cut-off value of 50%, the CT density values were not significantly different between the macrophage-rich plaques and the macrophage-poor plaques (69 ± 15 HU versus 64 ± 11 HU, $p = 0.294$). The correlation coefficients for the measurements of the lumen, vessel wall, and plaque area between the CTA and histopathologic results were 0.767, 0.783, and 0.739, respectively.

In conclusion, among the phases of 64-slice CTA, DP_{90s} imaging has the best diagnostic performance in the detection of aortic plaques and allows quantification of aortic plaques. However, further classification of non-calcified plaques into vulnerable or stable plaques by CT density measurements is not reliable.

Key words: Computed tomographic angiography (CTA); Atherosclerotic plaque; Composition; Quantification

Assessment of atherosclerotic plaques in a rabbit model by multi-phase contrast-enhanced CT angiography: comparison with histopathology

Jin Hur

Department of Medicine
The Graduate School, Yonsei University

(Directed by Professor Byoung Wook Choi)

I. Introduction

A number of investigations have suggested that plaque composition, plaque burden, and the progression of coronary atherosclerosis are important factors related to the risk of patients experiencing an adverse coronary event[1-4]. It has been known that lipid-rich plaques increase risk for a future coronary atherosclerotic event. Therefore, differentiation between fibrous and lipid-rich plaques may be clinically relevant.

The current gold standard imaging technique for atherosclerosis is X-ray contrast angiography, which provides high-resolution definition of the site and severity of luminal stenosis, without information on vessel wall

changes and plaque composition. Thus, it cannot differentiate between unstable and stable plaques and, therefore, it is unable to predict the risk of plaque rupture. In order to assess the presence, extent and composition of atherosclerotic lesions in patients, there is a clinical need for a non-invasive diagnostic imaging technique which can be used to assess the vulnerability of atherosclerotic plaques.

Magnetic resonance imaging (MRI) has already demonstrated its ability to noninvasively quantify and characterize atherosclerotic lesions at the preclinical and clinical level[5-7]. Atherosclerotic plaque characterization by MRI is generally based on the signal intensities and morphological appearance of the plaque on T1-weighted, proton-density-weighted and T2-weighted images as previously validated[8]. The advantages of MRI as compared to computed tomography (CT) are the lack of radiation exposure, and the avoidance of iodinated contrast media. However, it has several disadvantages compared to CT. The examination time is longer than CT and more expensive than CT. Furthermore, MRI has limited ability in the visualization of coronary arteries because of limited spatial resolution.

The current focus of experimental and clinical research which use noninvasive technique to characterize coronary atherosclerotic plaques involves the measurement of Hounsfield Unit (HU) value using contrast-enhanced CT angiography (CTA). Previous studies have shown that calcified plaques, fibrous plaques, and lipid-rich plaques show significant differences in their mean CT attenuation[8-12]. However, Pohle et al. reported that there is a substantial overlap of CT attenuation values between fibrous and lipid-rich

plaque[12].

The current generation of 64-slice scanners with sub-second rotation times and a dedicated cardiac reconstruction algorithm has the ability to acquire three-dimensional data acquisition for the heart, enabling the detailed visualization of coronary arteries[13-15]. Therefore, there has been a growing interest in the use of CTA for atherosclerosis imaging due to its high resolution, short imaging time, and ability to depict not only arterial calcification and luminal stenosis but also non-stenotic and non-calcified plaques, even in the coronary arteries.

Luminal enhancement of the vessel is required to visualize the non-calcified components of atherosclerotic plaques using CTA. However, it has been reported that the density measurements within plaques are highly influenced by luminal enhancement[16]. Recently, enhancement of atherosclerotic plaques has been observed on delayed-phase CT after the intravenous contrast administration[16-18]. Halliburton et al.[18] demonstrated that perfusion model further revealed the persistent enhancement of non-calcified plaque during a delayed contrast phase in the absence of luminal enhancement.

Rabbit model of atherosclerosis is a well established model in that the aortic lumen is a fixed structure of the order of 4-5 mm in diameter, which is similar in size to the human coronary arteries[19]. Rabbits fed cholesterol < 0.5% developed predominantly fibromuscular lesions, whereas those fed higher cholesterol concentrations develop macrophage and monocyte infiltrative intimal lesions. Macrophage/monocyte infiltration is a component of

early human atheromatous lesions, and fibromuscular elements are present in more advanced human lesions, providing some clinical analogy[19]. Using a combination of balloon injury of the aorta with a high cholesterol diet, a number of investigators have attempted to increase aortic lesion severity and shorten the time to lesion induction[20]. Lesions formed in this way often have a number of features of human atheroma, including a lipid core and a fibrous cap rich in smooth muscle cells.

Based on the results from a previous study[18], we hypothesized that we could differentiate between the fibrous and lipid-rich plaques using multi-phase CT if we used quantitative measurements for HU within the plaques, because fibrous plaques will reveal a higher CT attenuation value compared to lipid-rich plaques during the delayed phase scanning. Therefore, the aim of this study was to assess the capability of multi-phase CTA for the characterization and quantification of atherosclerotic plaques in comparison with histopathology in an experimental rabbit model.

II. Materials and methods

1. Animal Model of Atherosclerosis

The animal model selected for this study was the male New Zealand white rabbit (n = 12, weight 3.0 - 3.5 kg). Aortic atherosclerosis was induced by a combination of a high-cholesterol diet (0.3% cholesterol-enriched diet; Feedlab, Hanam, Korea) for 6 months and two times of aortic balloon denudation injury (at 1 week and 1 month after starting the high-cholesterol diet). After exposure of the iliac artery, 4-French Fogarty embolectomy catheter was advanced through the aorta just above the diaphragm level. Then, the catheter balloon was inflated using a total of 0.5 mL of the diluted contrast agent. The aortic denudation injury was performed three times from the diaphragm to the iliac bifurcation (abdominal aorta) (Fig. 1). All procedures were performed under general anesthesia using tiletamine (30 mg/kg, Zoletil; Virbac, France) and xylazine (10 mg/kg, Rompun; Bayer, Korea). The study protocol was approved by our Animal Care and Use Committee.

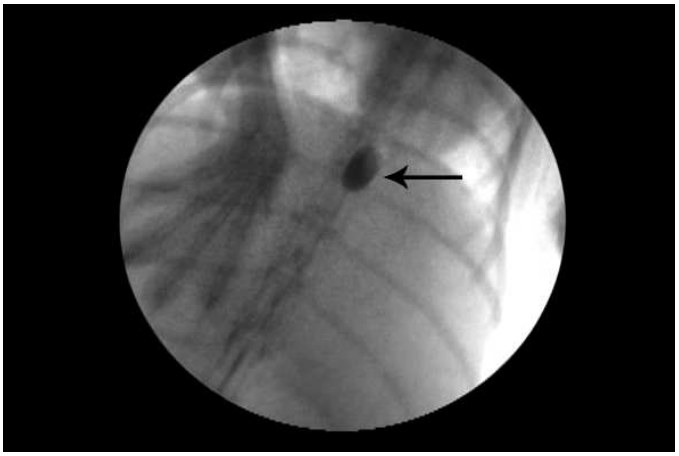

Figure 1. Aortic denuation injury in rabbit. Aortic denudation injury was performed with use of a 4F Fogarty embolectomy catheter three times from the diaphragm to the iliac bifurcation (abdominal aorta). Arrow indicate inflated balloon within the abdominal aorta.

2. Computed Tomography Angiography Examination

The CT angiography was performed using a 64-slice multi-detector computed tomography (MDCT) scanner (LightSpeed VCT XT, GE Healthcare). Intravenous access was placed in the central vein of the ear using a 21-gauge line.

For a contrast agent, we used a 1:2 dilution of the contrast agent (320 mg iodine/ml) with saline, yielding a concentration of 100-110 mg iodine per milliliter. This created intra-aortic lumen attenuation similar to that which is routinely obtained in human coronary artery CTA examinations (250

to 300 HU).

The animals were imaged in the cranio-caudal direction and in the supine position while they were under general anesthesia using intramuscular tiletamine (20 mg/kg, Zoletil; Virbac, France) and xylazine (5 mg/kg, Rompun; Bayer, Korea). The area of interest was the segment of the abdominal aorta immediately below the diaphragm to the iliac bifurcation.

The early phase (EP) scanning was started with a time delay that was determined using a real-time bolus-tracking technique. The region of interest (ROI) was established in the descending thoracic aorta to monitor a threshold of +100 HU above the baseline attenuation. The scans were started 4 sec after a threshold trigger of 100 HU was reached. A total of 15 mL of the contrast dilution was administered at a rate of 0.5 mL/s using an automated infusion pump (Medrad Envision CT, Medrad Inc).

Delayed phase (DP) scanning was started 90 sec (DP_{90s}) and 10 min later (DP_{10min}), after the completion of the EP scan. After those scans, 15 mL of saline was introduced at a rate of 0.5 mL/s and scanning was started 11 min later after the completion of the EP scan (DP_{Saline}: delayed phase scan with saline infusion).

The imaging parameters were set as follows: axial mode, collimation 0.625 mm × 64, 120 kV, 180 mA, and rotation time 0.5 s. The total acquisition time ranged from 14 to 17 sec. Axial images were reconstructed with a field of view of 160×160 mm, a 512×512 matrix, and a slice thickness of 0.625 mm with no overlap to allow direct comparison with histopathology sections.

3. Histopathology

The aortas were excised after the perfusion-fixation, which used 4% phosphate-buffered paraformaldehyde (4% in phosphate-buffered saline). Serial sections of the abdominal aorta were cut at 3-mm intervals to match the corresponding CTA images. Specimens were embedded in paraffin. A five-μm-thick section was taken from each top portion of each 3-mm pathology samples, and were stained with Masson's trichrome and Van Gieson's stain. The next five-μm-thick sections were additionally stained with a RAM-11 antibody which binds to macrophages (Dako, CA, USA). Aortic plaques are defined as structures of thickened aortic wall more than 1 mm which could be clearly distinguished from the vessel lumen and the surrounding tissue.

4. Comparison of CTA and Histopathology slices

The slices for each rabbit were numbered cranio-caudally to match the image slices in the two modalities (histopathology and CTA). Reconstructions of the 3 mm sections with no overlap were performed after acquisition of the images. We ensured concordance between the position of the CT slices and the corresponding histological slices using anatomical reference such as iliac bifurcation, right and left renal artery, superior mesenteric artery and celiac artery (Fig. 2).

For quantitative and qualitative plaque analysis, 2~4 consecutive 3-mm slices located above and including the celiac artery, 2~4 consecutive 3-mm slices below the celiac trunk and including the superior mesenteric artery and 5~6 consecutive 3-mm slices located below and including the left

renal artery were selected and were analyzed with the matching CT and histopathologic images.

After matching the CT image slices with the corresponding histopatholgy slices, each 3 mm sections of CT images were reconstructed into 0.625 mm sections with no overlap. We then compared every first slice of the histopathology slices (5 μm thick section) with the CT image slices (0.625 mm).

Figure 2. Matching the CT and the corresponding histopathological Hematoxylin & Eosin stained slices (Magnification x 12.5). The position of the CT slice and the corresponding histological slice was matched using anatomical reference such as renal artery (arrows).

5. Image Analysis of CTA

The CTA images were transferred to a dedicated workstation (Aquarius, TeraRecon, Inc; USA) for analysis. For all phases of CT imaging, we recorded the number of plaques that were detected.

After matching the CTA images with the corresponding histopathology slices, CT density measurements of the matched plaques were performed. In order to obtain the CT density measurements of the matched plaques, regions of interest (ROI) were manually placed inside the matched plaques. Two radiologists independently measured the tissue contrast at three randomly selected points in HU within the matched plaques. The mean HU values were used for analysis. Only density values determined in plaque areas that corresponded to plaques detected by histopathology was considered for retrospective calculation of density values of different plaque types. Therefore, we measured the CT attenuation values during each phase for the plaques that were detected on the CTA image. Two radiologists also independently measured the luminal enhancement of the aorta (HU values) from each section.

Luminal areas and total vessel cross-sectional areas (CSA) were traced manually. The plaque area was calculated by subtracting the luminal area from the vessel area. CT measurements of luminal and vessel wall CSA were performed using the DP_{90s} scan images, because this phase allowed detection of the largest number of aortic plaques compared to the other phases. Analysis of the CT images was completed by two blinded radiologists who reviewed the images in a random order. Mean values were used for the final analysis. The optimal image display setting was chosen on an individual

basis for plaque analysis and tissue differentiation. This setting typically had a window width between 400 HU and 700 HU and a level between 40 HU and 250 HU.

6. Image Analysis of Histopathology

The histopathologic sections were digitized to the same computer. An independent pathologist, who was blinded to the results of the CT, performed the histopathology analysis. Luminal areas and vessel areas were traced semi-automatically using a computer-assisted quantitative color image analysis system (Image Pro-Plus 6.3, MediaCybernetics). In our study, lipid rich areas, fibrous areas and calcified areas were also measured using the same analyzing software program (Image Pro-Plus 6.3, Media Cybernetics). On histopathologic sections, lipid rich areas were measured manually by drawing a loose matrix area where lipid laden macrophage were abundant on sections stained with Hematoxylin & Eosin. Fibrous areas were measured manually by drawing the dense pinkish area on sections stained with Hematoxylin & Eosin, which corresponds to blue area stained with Masson's trichrome stain. Calcified areas were measured manually by drawing in the empty space within the plaques that contain remaining remnant spotty crystal deposit stained violet on Hematoxylin & Eosin and Van Gieson's stain. Areas were expressed in mm^2. We considered a plaque to be lipid-rich if the percentage of lipid-rich area was over 50% of the total plaque area. Fibrous plaques were defined as having over 50% of fibrous area of the total plaque area. Mixed plaques were defined as having over 10% of calcified area of the total plaque area. Macrophage content was measured manually by drawing in

the brown area on sections stained with a RAM-11 antibody. The total macrophage area was normalized by dividing the total plaque area and was expressed as percentages. We defined a macrophage-rich plaque as having over 50% of macrophage stained area of the total plaque area.

7. Statistical Analysis

We calculated the sensitivity, specificity, and accuracy of CT for detecting plaques using histopathology as the reference standard.

The statistically significant differences in the CT densities of the plaques according to different plaque types determined by histopathology were assessed using a Student's t-test for independent samples. The statistically significant differences in the mean CT density of the fibrous and lipid-rich plaques according to different contrast CT phases were assessed using a one-way ANOVA with the Scheffe method. Correlations between the CT attenuation values of the plaques and the histological variables (the percentage of lipid-rich, fibrous and macrophage areas) were performed using a Pearson's correlation coefficient. Correlations between the CT measurements of the lumen CSA, vessel wall CSA, and plaque CSA with histopathologic results were performed using a Pearson's correlation coefficient. A Pearson's correlation was used to determine the correlation of mean values between the two observers. P-values less than 0.05 was considered statistically significant.

III. Results

A total of 110 non-calcified plaques (39 fibrous and 71 lipid-rich plaques) and 9 mixed plaques were identified from 232 sections on histopathology. There were no calcified plaques on histopathology. Using histopathology as the reference standard, the overall sensitivity, specificity and accuracy of 64-slice CTA for the detection of plaques was 59%, 100% and 79% for the EP scan, 88%, 100%, and 94% for the DP_{90s} scan, 81%, 100% and 90% for the DP_{10min} scan and 53%, 100% and 76% for the DP_{Saline} scan, respectively (Table 1) (Fig. 3).

Table 1. CT Results for Detection of Aortic Plaques Based on 119 Plaques from 232 Histopathologic Sections

Phase	EP[1]	DP_{90s}[2]	DP_{10min}[3]	DP_{Saline}[4]
True–Positive	70	105	96	63
True-Negative	113	113	113	113
False-Positive	0	0	0	0
False-Negative	49	14	23	56
Sensitivity (%)	59	88	81	53
Specificity (%)	100	100	100	100
Accuracy (%)	79	94	90	76

Note- 119 plaques include 110 non-calcified plaques and 9 mixed plaques.

[1]EP: Early-phase image

[2]DP_{90s}: Delayed-phase image 90 sec after contrast injection.

[3]DP_{10min}: Delayed-phase image 10min after contrast injection.

[4]DP_{Saline}: Delayed-phase image with saline infusion.

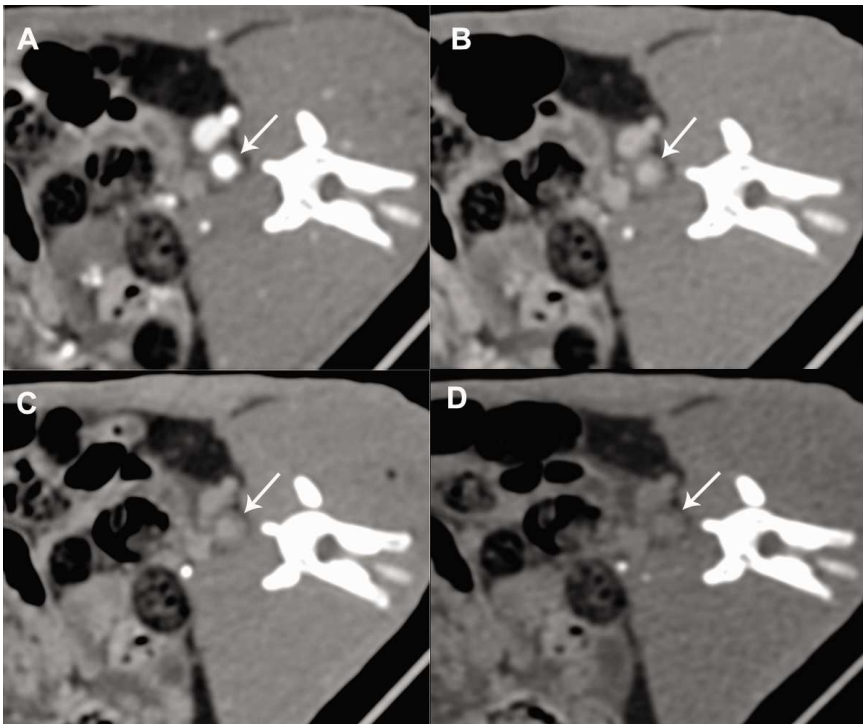

Figure 3. Detection of aortic plaques using multi-phase computed tomography angiography (CTA). (A) Early phase image. (B) Delayed phase image 90 sec after contrast injection (DP_{90s}). (C) Delayed phase image 10 min after contrast injection (DP_{10min}). (D) Delayed phase image with saline infusion (DP_{Saline}). The plaque (arrows) is easily detected on the DP_{90s} and DP_{10min} images.

Table 2. CT Density Measurements of Fibrous and Lipid-rich Plaques on Early- and Delayed-Phase Images

	Fibrous plaques	Lipid-rich plaques	P value
EP[1] (HU)	122 ± 21 (78 to 154)	113 ± 28 (65 to 148)	0.364
DP_{90s}[2] (HU)	83 ± 16 (35 to 105)	59 ± 19 (20 to 88)	0.005
DP_{10min}[3] (HU)	81 ± 17 (25 to 101)	63 ± 18 (24 to 80)	0.003
DP_{Saline}[4] (HU)	79 ± 10 (22 to 88)	60 ± 22 (23 to 81)	0.003

Note- range of measured CT attenuation values are in parentheses.

[1]EP: Where the CT density is measured during the early phase.

[2]DP_{90s}: Where the CT density is measured during the delayed phase 90 sec after contrast injection.

[3]DP_{10min}: Where the CT density is measured during the delayed phase 10 min after contrast injection.

[4]DP_{Saline}: Where the CT density is measured during the delayed phase with saline infusion.

The mean CT attenuation values of vessel lumen of each phase were 261 ± 9 HU (range, 231 to 315 HU) for EP images, 153 ± 7 HU (range, 141 to 164 HU) for DP_{90s} images, 118 ± 6 HU (range, 111 to 128 HU) for DP_{10min} images, and 84 ± 5 HU (range, 71 to 94 HU) for DP_{Saline} images, respectively. Because of the small number of mixed plaques, we measured the mean CT attenuation values only for non-calcified plaques. The mean CT attenuation values using the EP images for the fibrous and lipid-rich plaques were 122 ± 21 HU and 113 ± 28 HU, respectively (Table 2). The CT density measurements were not significantly different between the fibrous plaques and the lipid-rich plaques ($p = 0.364$). Using the DP_{90s} images, the mean CT attenuation values for the fibrous and lipid-rich plaques were 83 ± 16 HU and 59 ± 19 HU, respectively (Table 2) (Figs 4 and 5). The CT density measurements were significantly different between the fibrous plaques and the lipid-rich plaques ($p = 0.005$). The CT density measurements showed moderate correlations between the percentage of lipid and fibrous areas measured on histopathology ($r = -0.628$, and $r = 0.616$, respectively) (Figs 6A and 6B). Using the DP_{10min} images, the mean CT attenuation values for the fibrous and lipid-rich plaques were 81 ± 17 HU and 63 ± 18 HU, respectively (Table 2). The CT density measurements were significantly different between the fibrous plaques and the lipid-rich plaques ($p = 0.003$). The CT density measurements showed moderate correlations with the percentage of lipid and fibrous areas measured on histopathology ($r = -0.618$, and $r = 0.598$, respectively) (Figs 6C and 6D). After the saline infusion (DP_{Saline} scan), the mean CT attenuation values for the fibrous and lipid-rich plaques were 79 ± 10 HU and 60 ± 22 HU, respectively (Table 2). The CT

density measurements were significantly different between the fibrous plaques and the lipid-rich plaques ($p = 0.003$)

The mean CT attenuation values for the fibrous plaques and the lipid-rich plaques did not vary significantly among the different delayed contrast phases (DP_{90s}, DP_{10min}, and DP_{Saline}) ($p > 0.05$) (Table 2) (Fig. 7). The CT density measurements showed substantial overlap between the fibrous and lipid-rich plaques (Fig. 7).

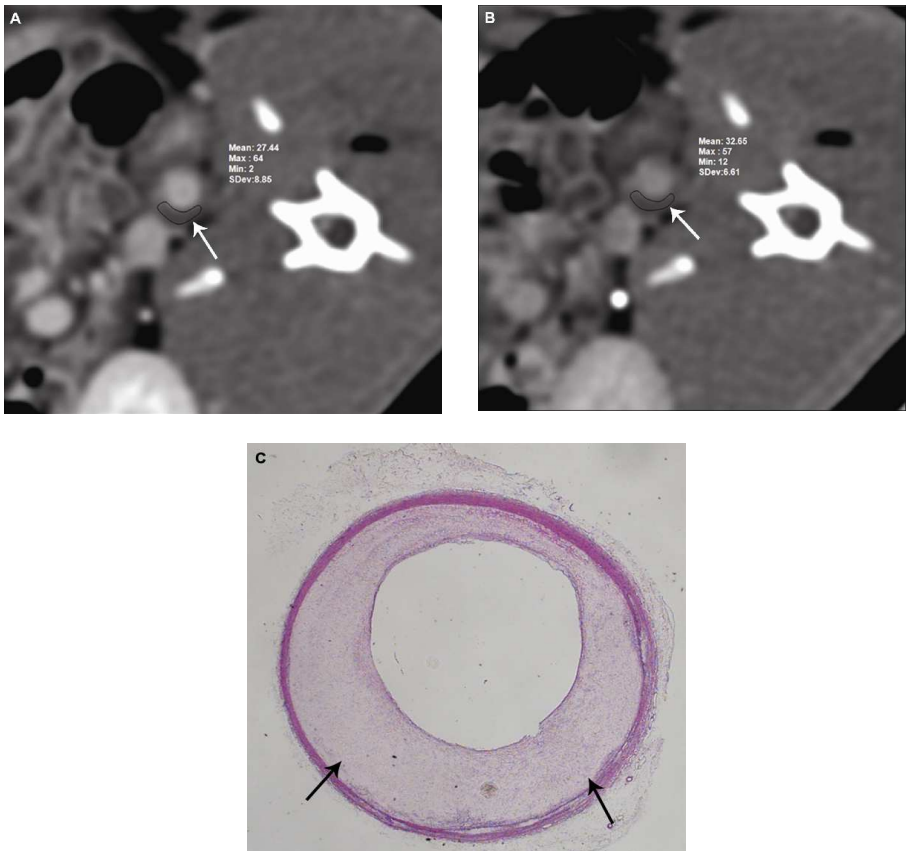

Figure 4. Lipid-rich plaque. (A) CT density measurement of the plaque (arrow) on DP_{90s} scan image. The mean CT attenuation value of the plaque was 27.4 HU. (B) CT density measurement of the plaque (arrow) on DP_{10min} scan image. The mean CT attenuation value of the plaque was 32.7 HU. (C) Corresponding histopathologic Hematoxylin & Eosin stained section (Magnification x 12.5). A lipid-rich plaque was defined if the percentage of lipid-rich area was over 50% of the total plaque area. The percentage of lipid-rich area (arrows) of the plaque was 82.4%.

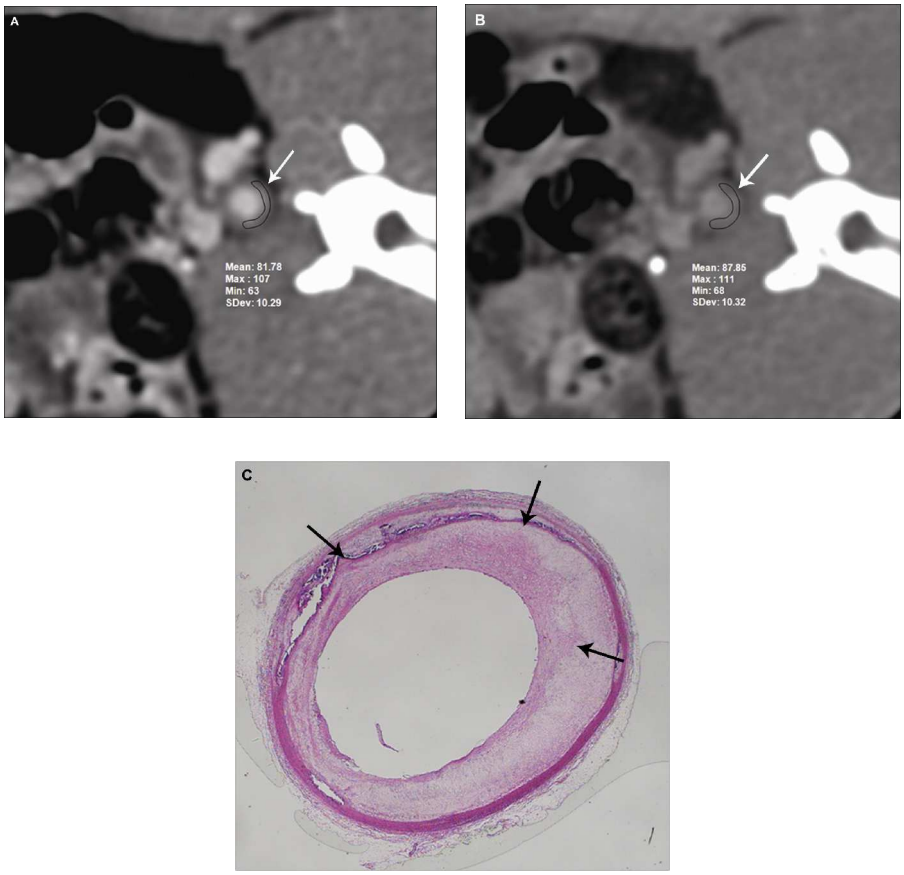

Figure 5. Fibrous plaque. (A) CT density measurement of the plaque (arrow) on DP_{90s} scan image. The mean CT attenuation value of the plaque was 81.8 HU. (B) CT density measurement of the plaque (arrow) on DP_{10min} scan image. The mean CT attenuation value of the plaque was 87.9 HU. (C) Corresponding histopathologic Hematoxylin & Eosin stained section (Magnification x 12.5). A fibrous plaque was defined as having over 50% of fibrous area of the total plaque area. The percentage of fibrous area of the plaque was 58.7%. Arrows indicate dense fibrous areas.

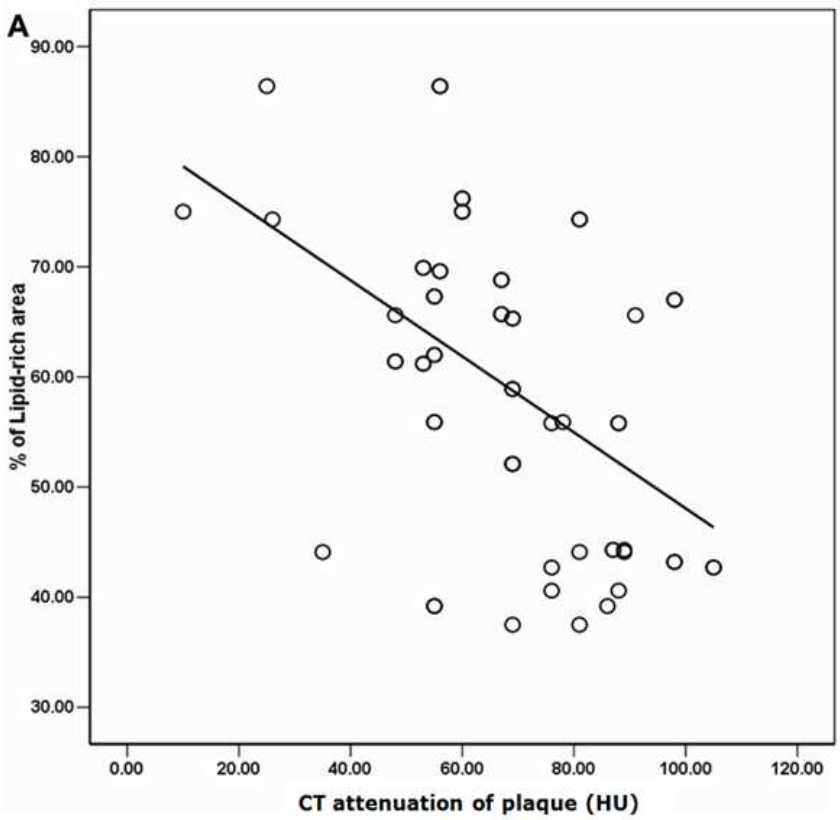

Figure 6A. Scatter plots of CT attenuation values. Correlation between the percentage of lipid-rich area and CT attenuation values (HU) of the plaques on DP_{90s} scan images. The correlation coefficient was -0.628. Regression line is drawn.

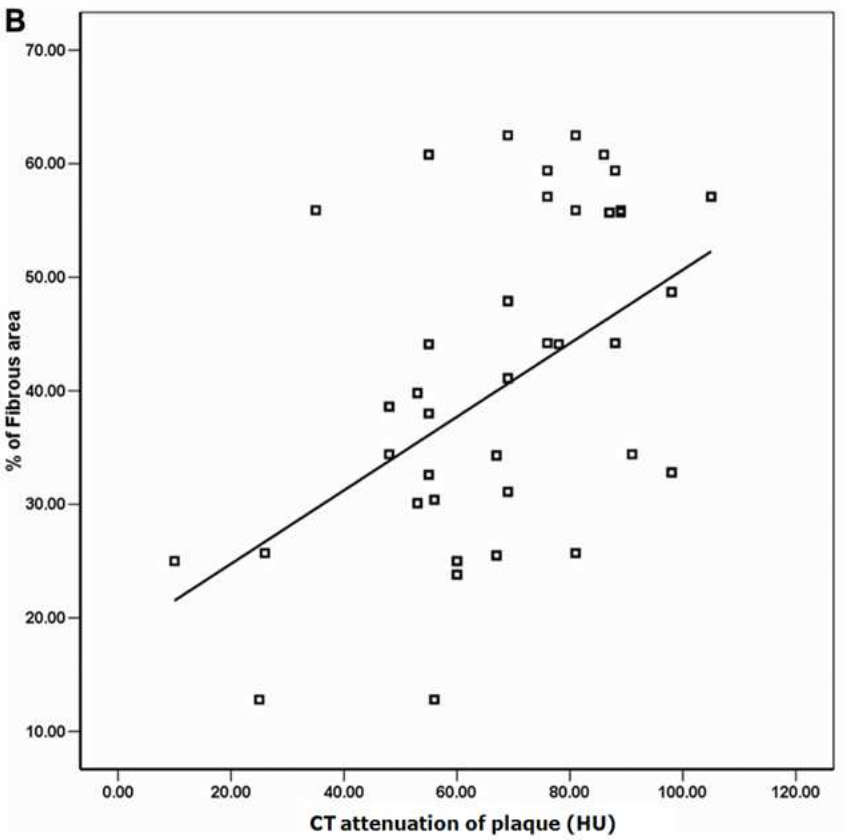

Figure 6B. Scatter plots of CT attenuation values. Correlation between the percentage of fibrous area and CT attenuation values (HU) of the plaques on DP_{90s} scan images. The correlation coefficient was 0.616. Regression line is drawn.

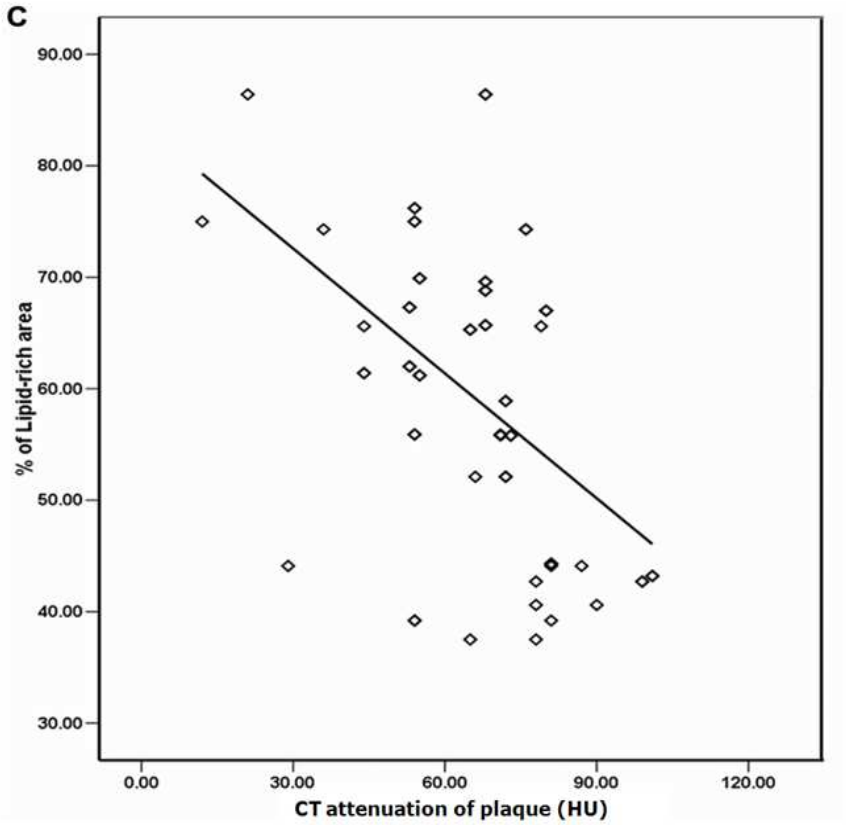

Figure 6C. Scatter plots of CT attenuation values. Correlation between the percentage of fibrous area and CT attenuation values (HU) of the plaques on DP_{10min} scan image. The correlation coefficient was -0.618. Regression line is drawn.

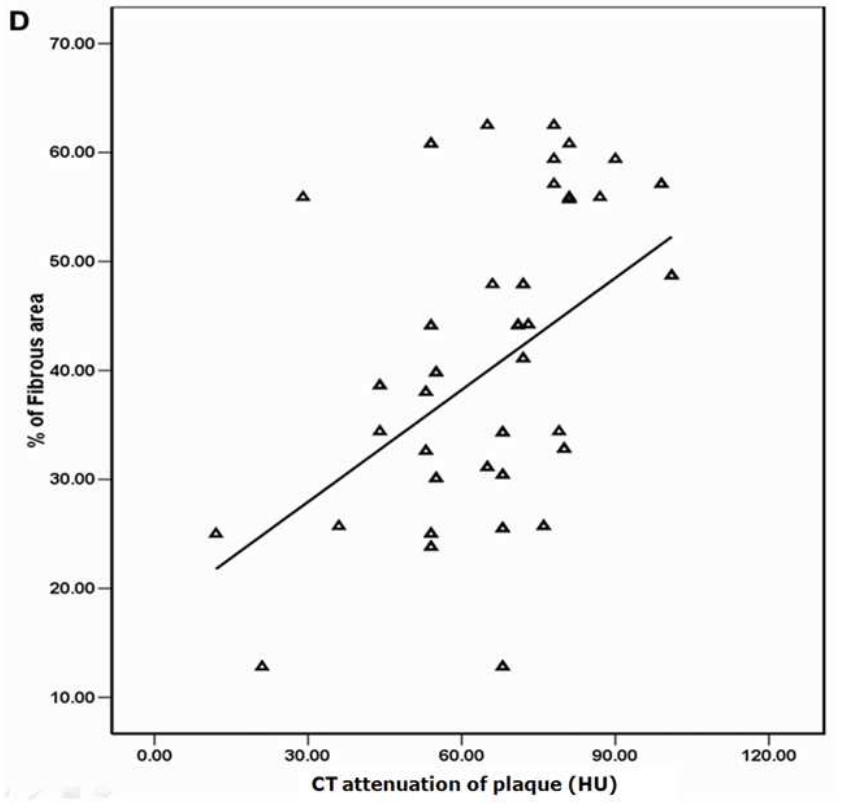

Figure 6D. Scatter plots of CT attenuation values. Correlation between the percentage of fibrous area and CT attenuation values (HU) of plaques on DP_{10min} scan image. The correlation coefficient was 0.598. Regression line is drawn.

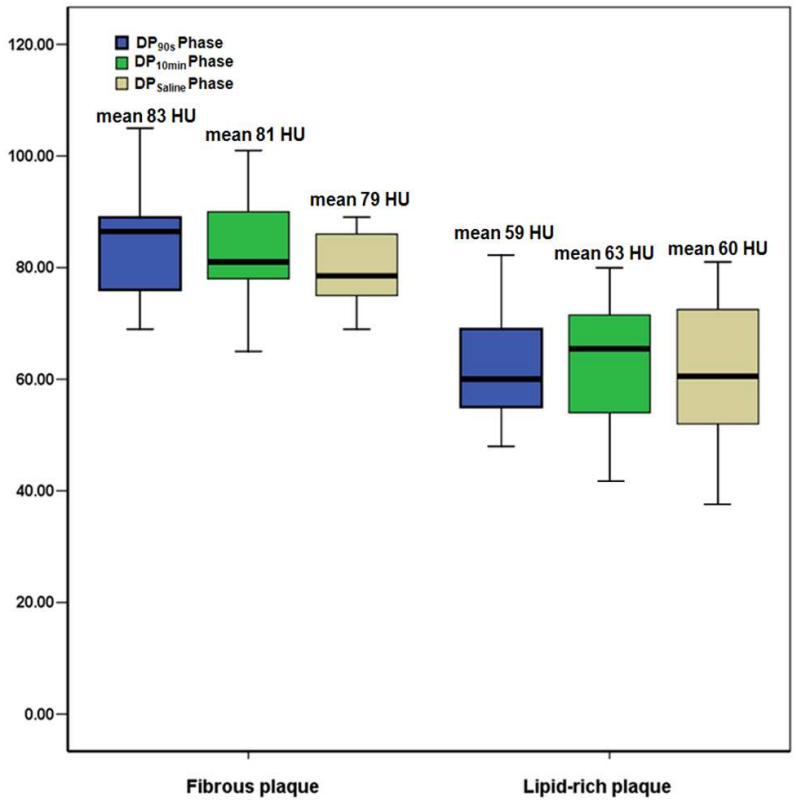

Figure 7. Box-whisker graph showing CT density values for the different delayed contrast phases (DP_{90s}, DP_{10min}, and DP_{Saline}) for the fibrous and lipid-rich plaques determined by histopathology. Each box describes the distribution of density values within one SD. DP_{90s} HU: Where HU is the CT density measured during the delayed phase image 90 sec after contrast injection. DP_{10min} HU: Where HU is the CT density measured during the delayed phase image 10 min after contrast injection. DP_{Saline}: Where HU is the CT density measured during the delayed phase image with saline infusion.

Using the DP_{90s} images, the percentage of macrophage areas was 43% ± 14 for the fibrous plaques and 51% ± 17 for the lipid-rich plaques. The percentage of macrophage areas was not significantly different between the fibrous plaques and the lipid-rich plaques (p = 0.138). When we divided aortic plaques into two groups according to the percentage of macrophage area using a cut-off value of 50%, the CT density values was not significantly different between the macrophage-rich plaques and the macrophage-poor plaques (n = 41, 69 ± 15 HU versus n = 69, 64 ± 11 HU, p = 0.294) (Figs 8 and 9). The mean CT density measurements showed poor correlations with the percentage of macrophage areas in both fibrous plaques and lipid-rich plaques (r = 0.408, and r = 0.333, respectively) (Fig. 10).

There was good inter-observer agreement and intra-observer agreement for the CT density values for the fibrous plaques and the lipid-rich plaques (r = 0.765, r = 0.744 and r = 0.818, r = 0.786, respectively).

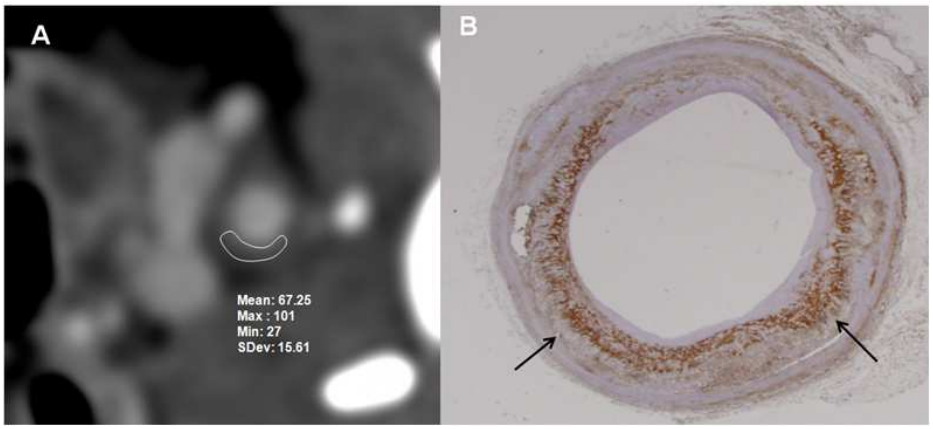

Figure 8. Macrophage-rich plaque. (A) CT density measurement of the plaque on DP_{90s} scan image. The mean CT attenuation value of the plaque was 67.3 HU. (B) Corresponding histopathologic RAM-11 stained section (Magnification x 12.5). Macrophage-rich plaque was defined if the percentage of macrophage stained area was over 50% of the total plaque area. The percentage of macrophage stained area of the plaque was 68.7%. Arrows indicate macrophage accumulation areas.

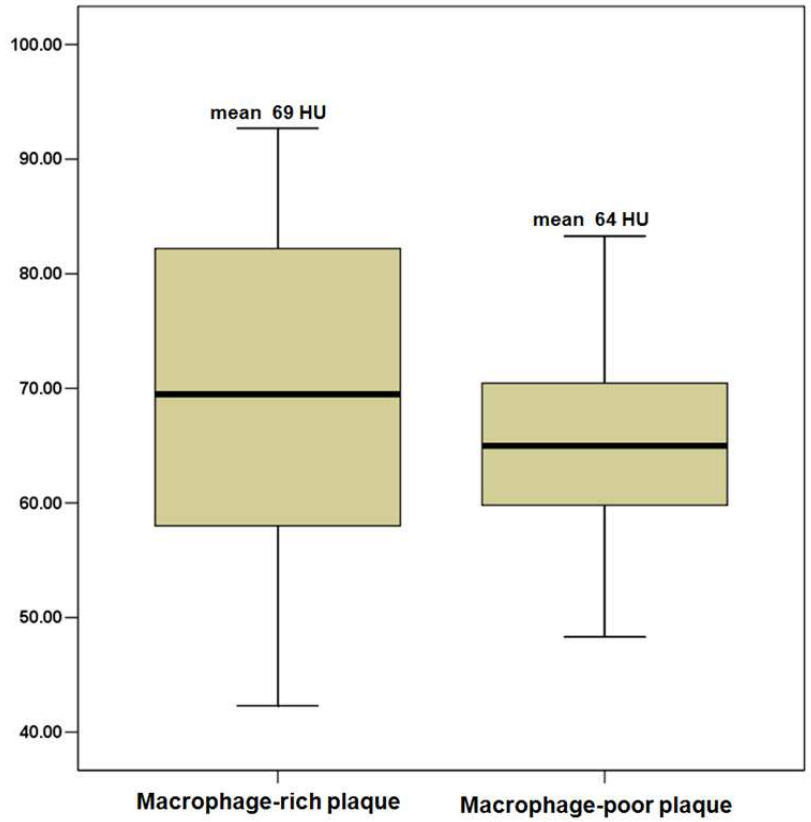

Figure 9. Box-whisker graph showing CT density values for the macrophage-rich plaques and the macrophage-poor plaques determined by histopathology. Each box describes the distribution of density values within one SD. We considered a plaque to be macrophage-rich if the percentage of macrophage area was over 50% of the total plaque area.

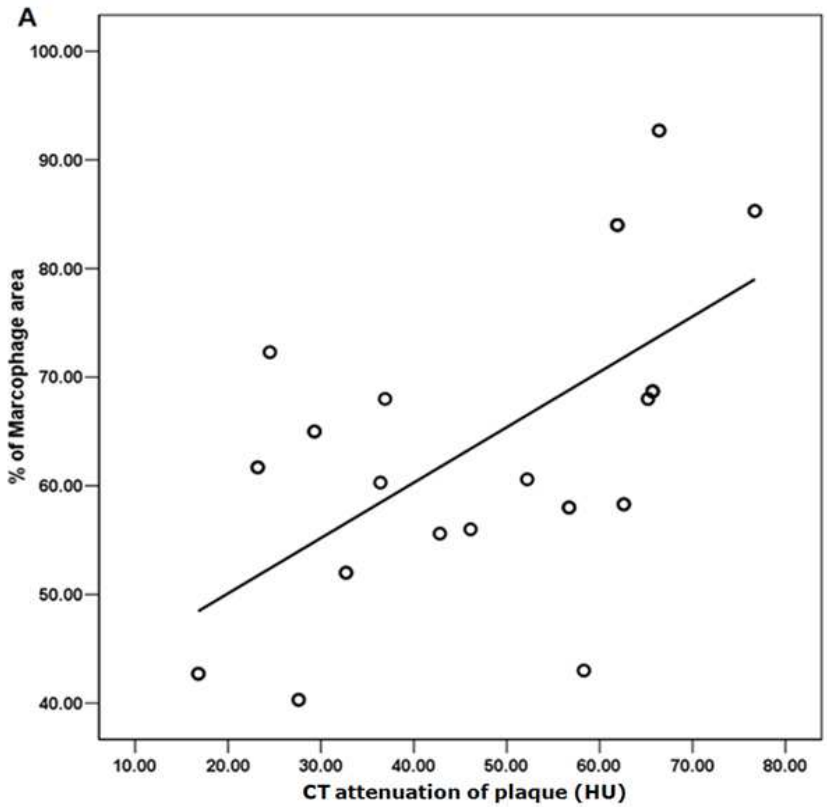

Figure 10A. Scatter plots of CT attenuation values measured on delayed-phase (DP_{90s}) image compared to the percentage of macrophage area for the fibrous plaque on histopathology exhibit poor correlation. The correlation coefficient was 0.408. Regression line is drawn.

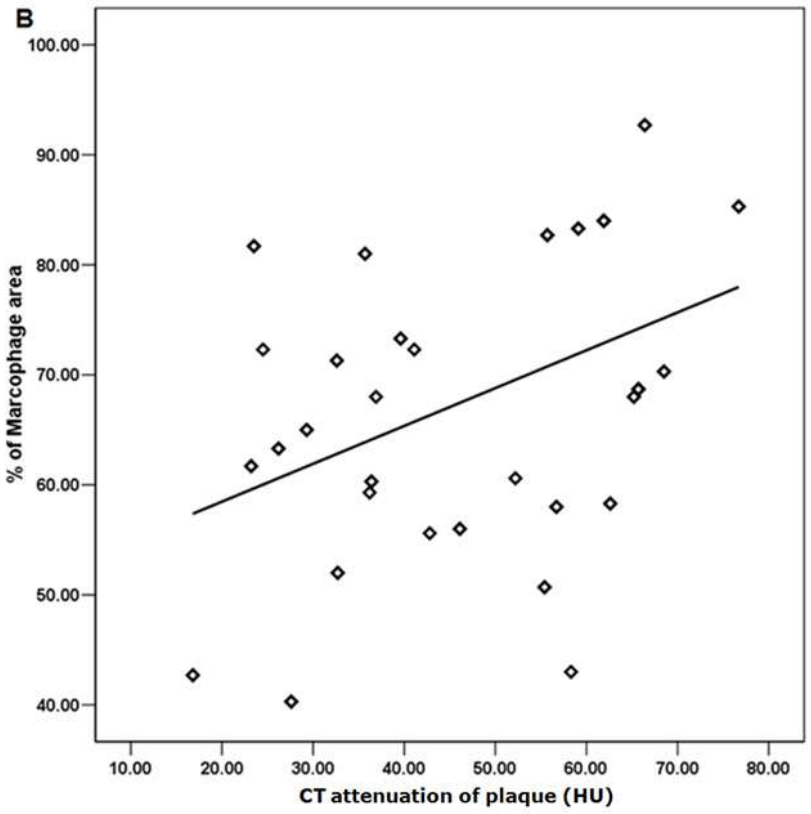

Figure 10B. Scatter plots of CT attenuation values measured on delayed-phase (DP_{90s}) image compared to the percentage of macrophage area for the lipid-rich plaque on histopathology exhibit poor correlation. The correlation coefficient was 0.333. Regression line is drawn.

Using the DP_{90s} scan CT, measurements from CTA and histopathology were 9.87 ± 1.64 mm^2 versus 7.72 ± 2.11 mm^2 (p = 0.001) for the mean lumen area, 23.94 ± 5.37 mm^2 versus 19.67 ± 5.52 mm^2 (p = 0.001) for the mean vessel wall area, 13.96 ± 2.04 mm^2 versus 11.47 ± 3.14 mm^2 (p = 0.032) for the mean plaque area and 1.26 ± 0.08 mm versus 1.22 ± 0.07 mm (p = 0.008) for the mean maximal plaque thickness (Table 3) (Fig. 11). These measurements were closely correlated (r = 0.762, r = 0.774, r = 0.713, and r = 0.707, respectively.) On average, the CTA results significantly overestimated lumen, vessel and plaque area compared to the histopathology results.

There was good inter-observer agreement for the CT measurements of the mean lumen areas, the mean vessel wall areas, the mean plaque areas and the mean maximal plaque thickness (r = 0.818, r = 0.736, r = 0.765, and r = 0.798, respectively).

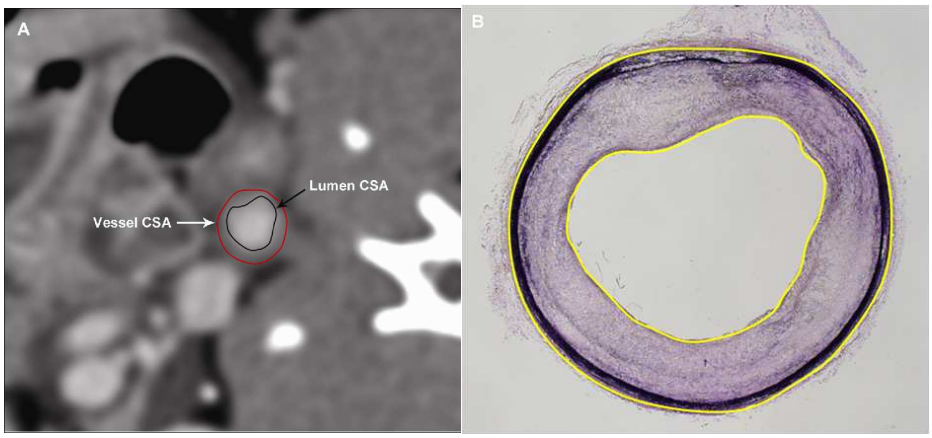

Figure 11. Measurements of lumen and vessel wall cross-sectional areas (CSA) using CTA and histopathology. (A) CTA cross-sectional image of an aortic plaque. Measurements of vessel wall CSA, lumen CSA, and plaque area were 21.13 mm^2, 8.16 mm^2 and 12.97 mm^2, respectively. (B) Cross-sectional image of the histopathological section stained with Van Gieson's stain on the corresponding level of image A (Magnification x 12.5). Measurements of the vessel wall area, lumen area and plaque area were 18.25 mm^2, 6.69 mm^2, and 11.56 mm^2, respectively. CSA = cross-sectional area.

Table 3. Comparison of CT Angiography (CTA) and Histopathology for the Quantification of Aortic Atherosclerotic Plaques

	CTA	Histopathology	CTA vs Pathology
Lumen CSA (mm^2)	9.87 ± 1.64	7.72 ± 2.11	r^a=0.762, p^b=0.001
Vessel wall CSA (mm^2)	23.94 ± 5.37	19.67 ± 5.52	r^a=0.774, p^b=0.001
Plaque area (mm^2)	13.96 ± 2.04	11.47 ± 3.14	r^a=0.713, p^b=0.032
Max thickness (mm)*	1.26 ± 0.08	1.22 ± 0.14	r^a=0.707, p^b=0.008

Note- CT measurements of lumen, vessel wall, plaque CSA and maximal plaque thickness were performed on the DP_{90s} scan images.

CSA: cross-sectional area

CTA: Computed Tomography Angiography

*Max thickness: maximal plaque thickness

[a]Pearson's correlation coefficient.

[b]Student's t-test for independent samples.

IV. Discussion

Accurate *in vivo* imaging, especially of the coronary artery vessel walls remains challenging using 64-slice CTA. However, there is a growing interest in the use of MDCT for atherosclerosis imaging due to its high resolution, short imaging time, and the ability to depict the presence and morphology of non-stenotic, non-calcified plaques, even in the coronary arteries[13, 14].

Correct opacification of the vessel lumen and optimization of the vessel contrast-to-noise ratio is essential for an optimal delineation of atherosclerotic plaques[16, 21]. Nikolaou et al. reported that a target attenuation of 250 HU is best suited to fulfill these requirements[21]. However, in our study, EP images which had an attenuation between 231 - 315 HU in the lumen had a low sensitivity (59%) for the detection of aortic plaques. The DP_{90s} images, which had an attenuation between 141 - 164 HU in the lumen showed the highest sensitivity (88%) and highest accuracy (94%) for the diagnosis of aortic plaques compared to histopathology. These finding suggests that a single phase CTA protocol is not sufficient for the detection of plaques, because the high contrast enhancement in the lumen has a significant influence on the evaluation of atherosclerotic plaques on the vessel wall.

Recently, Halliburton et al. demonstrated that the mean CT attenuation values of the vessel wall during and after contrast injection exceeded the mean CT attenuation values before injection for non-calcified plaques including both fibrous and fibrofatty plaques[18]. This observation suggests that non-calcified plaques demonstrate a persistent enhancement

during a delayed contrast phase scan. Therefore, we hypothesized that a delayed scan may enable differentiation between the fibrous and lipid-rich plaques by using a quantitative measurement of CT attenuation values. This is because a fibrous plaque will demonstrate a higher CT attenuation values compared to lipid-rich plaque with delayed phase scanning.

The determination of tissue density, expressed in HU units, is a standard technique with CT imaging and is used as a surrogate marker for tissue composition. However, density measurements within plaques are highly dependent on lumen enhancement[17]. Cademartiri et al. reported that the mean attenuation of coronary plaque increased with increasing attenuation of the lumen[17]. In our study, the CT density measurements based on the EP images were not significantly different between the fibrous plaques and the lipid-rich plaques. However, previous studies using human coronary arteries plaques have shown that fibrous plaques and lipid-rich plaques show significant differences in their mean CT attenuation using similar protocol with EP images[9-11]. These different results may be explained by the different plaque morphology and size between the human coronary artery plaques and rabbit aorta plaque. First, majority of aortic plaques in rabbit showed diffuse aortic wall thickening, in contrast to human coronary artery plaque, which was more localized in their morphology. Second, the size of the plaques in the rabbit was smaller than human coronary plaques. Therefore, in this situation, we expect that higher density of contrast opacification in the vessel lumen will negatively influence accurate contrast measurement for smaller and diffuse plaques.

In our study, the CT density measurements based on the DP_{90s},

DP_{10min} and DP_{Saline} images were significantly different between the fibrous plaques and the lipid-rich plaques. However, the CT density measurements showed a substantial overlap between the fibrous and lipid-rich plaques during all three of these different delayed phases. Furthermore, the mean CT density values for the fibrous plaques and the lipid-rich plaques were similar in each of the contrast phases. This quantitative analysis suggests that delayed phase imaging, with or without saline infusion does not help for differentiating between fibrous and lipid-rich plaques. We believe that CT attenuation values are insufficient for the accurate characterization of the heterogeneous plaque composition.

By previous studies, it was reported that macrophages contribute extensively to the development of inflammation in plaques and ruptured plaques have large numbers of macrophages[22, 23]. In our study, we correlated between the CT density values and the percentage of macrophage area on histopathology. However, the mean CT density measurements showed poor correlations with the percentage of macrophage areas in both fibrous plaques and lipid-rich plaques. This finding suggests that CT attenuation value dose not correlate with the intensity of macrophage infiltration on histology. Therefore, we think that CT attenuation values are insufficient to reflect the inflammatory activity in the plaque.

Several studies have investigated the diagnostic accuracy of CTA for the quantification of coronary artery plaques[24-26]. Leber et al. studied 32 coronary arteries using intravascular ultrasound (IVUS) and compared the mean plaque areas and the percentage of vessel obstruction to measurements made using a 64-slice CT[25]. In their study, the mean plaque area measured

using IVUS was 8.1 mm^2. The mean area was 7.3 mm^2 using a 64-slice CT ($p < 0.03$, $r = 0.73$). Our results were similar. In our study, we attempted to find correlations between the values for the maximal lumen, vessel, and plaque areas obtained by CTA and histopathology. The correlations of these measurements were good. However, on average, CTA systematically and significantly overestimated lumen, vessel and plaque area compared to results obtained by histopathology. We think that the missing blood pressure and the shrinkage of tissue caused by formalin fixation may lead to an underestimation of plaque size in histopathology.

There are some limitations to this study. First, histopathology examination was used as the gold standard for the assessment of the multi-phase CTA findings. However, the processing of samples for examination by histopathology results in the shrinkage of the specimen and makes a comparison of absolute values difficult. In addition, some variability arises due to differences in slice thickness in the z direction on CT and histology. Second, abdominal aortic lesions were induced in a well established rabbit model for atherosclerosis[27]. However, the size and composition of atherosclerotic plaques in this experimental rabbit model are different from complex atherosclerotic plaques in humans. Human atheroma, in contrast to rabbit model, progresses toward plaque vulnerability and rupture, which is important in the clinical situations[19, 28]. Another limitation is radiation exposure. The use of CT involves exposure to X-ray radiation and iodinated contrast agent.

V. Conclusion

Our study results show that DP_{90s} imaging using a multi-phase 64-slice CTA has the best diagnostic performance for the detection of aortic plaques. However, delayed phase imaging had little value for the differentiation between fibrous and lipid-rich plaques. These results suggest that classification of non-calcified plaques into vulnerable or stable plaques by CT density measurements is not reliable and current single CTA protocol is insufficient for the evaluation of lipid-rich atherosclerotic plaques.

References

1. Waxman S. Characterization of the unstable lesion by angiography, angioscopy, and intravascular ultrasound. Cardiol Clin 1999;17:295–305.

2. Virmani R, Burke AP, Kolodgie FD, Farb A. Vulnerable plaque: the pathology of unstable coronary lesions. J Interv Cardiol 2002;15:439–46.

3. Kolodgie FD, Burke AP, Farb A, Gold HK, Yuan J, et al. Thin-cap fibroatheroma: a type of vulnerable plaque: the major precursor lesion to acute coronary syndromes. Curr Opin Cardiol 2001;16:285–92.

4. Goldstein JA, Demetriou D, Grines CL, Pica M, Shoukfeh M, O'Neill WW. Multiple complex coronary plaques in patients with acute myocardial infarction. N Engl J Med 2000;343:915–22.

5. Helft G, Worthley SG, Fuster V, Zaman AG, Schechter C, Osende JI, et al. Atherosclerotic aortic component quantification by noninvasive magnetic resonance imaging: an in vivo study in rabbits. J Am Coll Cardiol 2001;37:1149–54.

6. Helft G, Worthley SG, Fuster V, Fayad ZA, Zaman AG, Corti R, et al. Progression and regression of atherosclerotic lesions: monitoring with serial non-invasive magnetic resonance imaging. Circulation 2002;105:993–98.

7. Skinner MP, Yuan C, Mitsumori L, Hayes CE, Raines EW, Nelson JA, et al. Serial magnetic resonance imaging of experimental atherosclerosis detects lesion fine structure, progression and complications in vivo. Nat Med 1995;1:69–73.

8. Fayad ZA, Fuster V. Clinical imaging of the high-risk or vulnerable atherosclerotic plaque. Circ Res 2001;89:305–16.

9. Caussin C, Ohanessian A, Ghostine S, Jacq L, Lancelin B, Dambrin G, et al. Characterization of vulnerable non stenotic plaque with 16-slice computed tomography compared with intravascular ultrasound. Am J Cardiol 2004;94:99–104.

10. Schroeder S, Kopp AF, Baumbach A, Meisner C, Kuettner A, Georg C, et al. Noninvasive detection and evaluation of atherosclerotic coronary plaques with multislice computed tomography. J Am Coll Cardiol 2001;37:1430–35.

11. Leber AW, Knez A, Becker A, von Ziegler F, Nikolaou K, Rist C, et al. Accuracy of multidetector spiral computed tomography in identifying and differentiating the composition of coronary atherosclerotic plaques: a comparative study with intracoronary ultrasound. J Am Coll Cardiol 2004;43:1241–47.

12. Pohle K, Achenbach S, Macneill B, Ropers D, Ferencik M, Moselewski F, et al. Characterization of non-calcified coronary atherosclerotic plaque by multi-detector row CT: comparison to IVUS. Atherosclerosis 2007;190:174-80.

13. Nikolaou K, Flohr T, Knez A, Rist C, Wintersperger B, Johnson T, et al. Advances in cardiac CT imaging: 64-slice scanner. Int J Cardiovasc Imaging 2004;20:535–40.

14. Raff GL, Gallagher MJ, O'Neill WW, Goldstein JA. Diagnostic accuracy of noninvasive coronary angiography using 64-slice spiral computed tomography. J Am Coll Cardiol 2005;46:552–57.

15. Mollet NR, Cademartiri F, van Mieghem CA, Runza G, McFadden EP,

Baks T, et al. High-resolution spiral computed tomography coronary angiography in patients referred for diagnostic conventional coronary angiography. Circulation 2005;112:2318–23.

16. Schroeder S, Flohr T, Kopp AF, Meisner C, Kuettner A, Herdeg C, et al. Accuracy of density measurements within plaques located in artificial coronary arteries by X-ray multislice CT: results of a phantom study. J Comput Assist Tomogr 2001;25:900–6.

17. Cademartiri F, Mollet NR, Runza G, Bruining N, Hamers R, Somers P, et al. Influence of intracoronary attenuation on coronary plaque measurements using multislice computed tomography: observations in an ex vivo model of coronary computed tomography angiography. Eur Radiol 2005;15:1426-31.

18. Halliburton SS, Schoenhagen P, Nair A, Stillman A, Lieber M, Murat Tuzcu E, et al. Contrast enhancement of coronary atherosclerotic plaque: a high-resolution, multidetector-row computed tomography study of pressure-perfused, human ex-vivo coronary arteries. Coron Artery Dis 2006;17:553-60.

19. McMahon AC, Kritharides L, Lowe HC. Animal models of atherosclerosis progression: current concepts. Curr Drug Targets Cardiovasc Haematol Disord 2005;5:433–40.

20. Abela GS, Picon PD, Friedl SE, Gebara OC, Miyamoto A, Federman M, et al. Triggering of plaque disruption and arterial thrombosis in an atherosclerotic rabbit model. Circulation 1995;91:776-84.

21. Nikolaou K, Becker CR, Flohr T, Huber A, Scheidler J, Fayad ZA, et al. Optimization of ex vivo CT- and MR- imaging of atherosclerotic vessel wall

changes. Int J Cardiovasc Imaging 2004;20:327-34.

22. Libby P. Inflammation in atherosclerosis. Nature 2002;420:868-74.

23. van der Wal AC, Becker AE, van der Loos CM, Das PK. Site of intimal rupture or erosion of thrombosed coronary atherosclerotic plaques is characterized by an inflammatory process irrespective of the dominant plaque morphology. Circulation 1994;89:36-44.

24. Moselewski F, Ropers D, Pohle K, Hoffmann U, Ferencik M, Chan RC, et al. Comparison of measurement of cross-sectional coronary atherosclerotic plaque and vessel areas by 16-slice multidetector computed tomography versus intravascular ultrasound. Am J Cardiol 2004;94:1294–97.

25. Leber AW, Knez A, von Ziegler F, Becker A, Nilolaou K, Paul S, et al. Quantification of obstructive and non-obstructive coronary lesions by 64-slice computed tomography; A comparative study with quantitative coronary angiography and intravascular ultrasound. J Am Coll Cardiol 2005;46:147–54.

26. Leber AW, Becker A, Knez A, von Ziegler F, Sirol M, Nikolaou K, et al. Accuracy of 64-slice computed tomography to classify and quantify plaque volumes in the proximal coronary system; A comparative study using intravascular ultrasound. J Am Coll Cardiol 2006;47:672–77.

27. Viles-Gonzalez JF, Poon M, Sanz J, Rius T, Nikolaou K, Fayad ZA, et al. In vivo 16-slice, multidetector row computed tomography for the assessment of experimental atherosclerosis: comparison with magnetic resonance imaging and histopathology. Circulation 2004;110:1467–72.

28. Bengel FM. Atherosclerosis imaging on the molecular level. J Nucl Cardiol 2006;13:111–18.

<Abstract (in korean)>

다중주기 조영증강 다중검출기 컴퓨터단층촬영을 이용한 동맥경화반의 평가: 토끼 모델에서의 조직병리와 비교한 실험적 연구

지도 교수: 최 병 욱

연세대학교 대학원 의학과

허 진

동맥경화반을 발견하고 성분을 정확하게 분석할 수 있는 비침습적인 영상기법이 임상적으로 필요한 실정이다. 최근에 조영제 주입 후에 동맥경화반이 조영증강을 보인다는 연구 결과가 발표 되었다. 따라서 본 연구는 토끼 모델에서의 동맥경화반 평가에서 다중주기 조영증강 다중검출기 컴퓨터단층촬영(CT)의 유용성을 조직병리와 비교하여 조사하고자 하였다.

12 마리의 토끼 동맥경화반 모델을 이용하여 복부대동맥에서 다중주기 조영증강 컴퓨터단층촬영을 시행하였다. 영상 촬영 방법은 초기영상 (EP), 조영제 주입 90초 후의 지연기 영상 (DP_{90s}), 조영제 주입 10분 후의 지연기 영상 (DP_{10min}), 그리고 생리식염수 주입 후의 지연기 영상 (DP_{Saline})을 촬영하였다. 동맥경화반의 성분은 조직병리 소견에서의 지방 성분 및 섬유성 성분의 비율과 컴퓨터 단층촬영에서의 CT 밀도 측정을 통하여 분석하였다. 각각의 경화반에서 최대 총 혈관면적,

최대 내강면적 그리고 경화반의 최대 면적을 측정하였다. 컴퓨터단층촬영의 측정 결과와 조직병리의 측정 결과의 일치도를 Pearson계수를 이용하여 분석하였다.

조직병리에서 발견된 119개의 동맥경화반을 기준으로 다중 주기 조영 증강 컴퓨터단층촬영의 경화반 발견에 있어서의 민감도, 특이도, 그리고 정확도는 초기영상 (EP scan)에서 각각 59%, 100%, 79%였고, 조영제 주입 90초 후 지연기 영상 (DP_{90s})에서 각각 88%, 100%, 94%였다. 조영제 주입 10분 후 지연기 영상 (DP_{10min})에서는 각각 81%, 100%, 90%였으며 생리식염수 주입 후의 지연기 영상 (DP_{Saline})에서 각각 53%, 100%, 76%였다. 조직 병리 소견을 기준으로 나눈 지방풍부 경화반과 섬유성 경화반에서 CT 밀도 측정값이 통계적으로 유의한 차이를 보였다 ($p < 0.05$). 그러나 각 성분의 CT 밀도 측정값이 넓은 범위에 걸쳐 있어서 지방풍부 경화반과 섬유성 경화반 간에는 서로 겹치는 범위가 존재하였다. 조직병리에서의 대식세포의 염색 범위를 50%를 기준으로 대식세포 풍부 경화반과 대식세포 빈약 경화반을 구별하였을 경우 CT 밀도 측정값은 통계적으로 큰 차이가 없었다(69 ± 15 HU vs 64 ± 11 HU, $p = 0.294$). 조직병리와 컴퓨터단층촬영에서의 총 혈관면적, 내강면적 그리고 경화반의 면적측정의 일치도는 각각 $r = 0.767$, $r = 0.783$, 그리고 $r = 0.739$였다.

결론적으로 이번 연구에 의하면 다중주기 조영증강 컴퓨터단층촬영 중 조영제 주입 90초 후의 지연기 영상 (DP_{90s})이 동맥경화반의 발견과 정략적 분석에 가장 유용함을 알 수 있었다. 그러나 지연기 영상을 추가하더라도 CT 밀도 측정을 통한 지방풍부 경화반과 섬유성 경화반의 정확한 감별에는 한계가 있음을 알 수 있었다.

핵심 되는 말: 컴퓨터 전산화 단층촬영 (CT), 동맥 경화반, 성분, 정량적 분석